Polar Pore Surface of Polyamide Membranes Enabling Efficient Solvent Mixture Separation

Zhang, Aiwen ; Guan, Kecheng ; Mai, Zhaohuan ; Wang, Zheng ; Dai, Liheng ; Li, Chuang ; Li, Bowen ; Li, Zhan ; Hu, Mengyang ; Zhang,…

(Citation)
Advanced Functional Materials,35(23):2422376

(Issue Date)
2025-06-05

(Resource Type)
journal article

(Version)
Version of Record

ADVANCED FUNCTIONAL MATERIALS
www.afm-journal.de

Polar Pore Surface of Polyamide Membranes Enabling Efficient Solvent Mixture Separation

Aiwen Zhang, Kecheng Guan, Zhaohuan Mai, Zheng Wang, Liheng Dai, Chuang Li, Bowen Li, Zhan Li, Mengyang Hu, Pengfei Zhang, and Hideto Matsuyama**

Separating solvent mixtures without phase change using polyamide membranes reduces energy consumption and enhances environmental sustainability. However, overemphasizing precise pore control while neglecting membrane–solvent interactions hinder membrane development and reduces separation efficiency. Here, it is demonstrated that rapid separation of solvents of differing polarity can be achieved using a polyamide membrane featuring relatively large pores with a polar surface formed via interfacial polymerization between polyethyleneimine (PEI) and trimesoyl chloride (TMC). The abundant amine groups and flexible chains of PEI facilitate the formation of a polyamide network that enables fast and selective transport of mixed solvents with varying polarity. The membrane can exhibit several-fold-higher permeance while maintaining comparable permselectivity compared to conventional polyamide membranes fabricated from the reaction of *m*-phenylenediamine with TMC. This work leverages membrane–solvent interactions to achieve solvent mixture differentiation and may guide the development of high-performance polymer membranes for efficient solvent mixture separation.

1. Introduction

Separating solvent mixtures is essential for recovering resources and purifying products in industries such as chemicals, pharmaceuticals, and petroleum.[1] Currently, the primary method for purifying solvent mixtures mainly relies on energy-intensive distillation processes, which currently account for 10%–15% of global energy consumption.[2] Pressure-driven membrane separation with high energy efficiency offers a promising alternative to thermal processes by differentiating molecules based on size, conformation, and interactions without phase change. Membrane technologies have become well-established for water purification (e.g., desalination), and have recently emerged for solute removal from organic solvents (organic solvent nanofiltration, OSN). However, their application in organic media (e.g., organic solvent reverse osmosis) remains underexplored due to the complexity of solvent mixtures.[1b] Nowadays, a major challenge in developing membranes for separating solvent mixtures is their generally low permeance.[3] Organic solvent molecules typically have similar molecular sizes, and relying on precise size sieving of membranes to enhance selectivity inevitably sacrifices permeance.[4] Moreover, precisely controlling membrane pore size is technically challenging and limits separation targets.[5] This necessitates exploring other strategies beyond pore size sieving to further enhance the separation performance for solvent mixtures.

Within limited pore space, interactions between the pore surface and transporting molecules can affect molecular transport significantly. Modifying the pore surface chemistry of the membranes thus alters membrane–solvent interactions (e.g., affinity and repulsion) and can change solvent transfer behavior. This means that the modulation of membrane pore structure is governed by the properties of the solvents, such as molecular size, polarity, and dielectric constant.[6] Statistical results indicate that most organic solvents have a narrow molecular size range of 0.55–0.8 nm,[7] but exhibit distinct polarities (**Figure 1a**; Table S1, Supporting Information). Polarity, a fundamental solvent parameter, varies more among different solvents, making it an effective criterion for solvent molecule differentiation.[6a,8] According to the principle of "like dissolves like",[9] membrane materials with high polarity enhance affinity toward polar molecules while repelling nonpolar ones. Thus, membranes with a suitably limited pore size and polar pore surface can facilitate the transport of higher-polarity solvent molecules while hindering lower-polarity ones, thereby achieving effective solvent

A. Zhang, K. Guan, Z. Mai, Z. Wang, L. Dai, C. Li, B. Li, Z. Li, M. Hu, P. Zhang, H. Matsuyama
Research Center for Membrane and Film Technology
Kobe University
1-1 Rokkodaicho, Nada, Kobe 657–8501, Japan
E-mail: guan@people.kobe-u.ac.jp; matuyama@kobe-u.ac.jp
A. Zhang, Z. Wang, C. Li, B. Li, H. Matsuyama
Department of Chemical Science and Engineering
Kobe University
1-1 Rokkodaicho, Nada, Kobe 657–8501, Japan
The ORCID identification number(s) for the author(s) of this article can be found under https://doi.org/10.1002/adfm.202422376

DOI: 10.1002/adfm.202422376

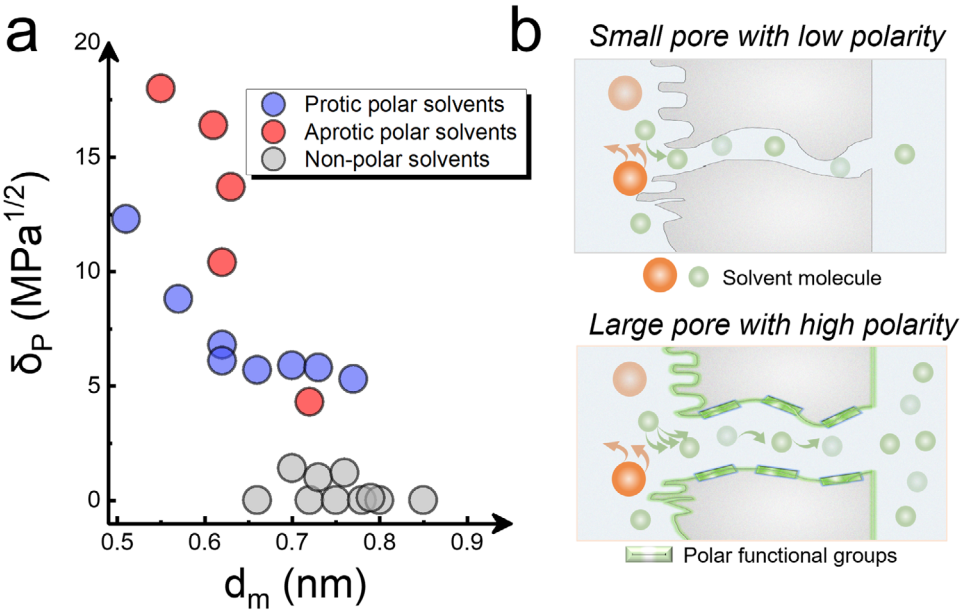

Figure 1. a) Distribution diagram of molar diameters (d_m, nm) and Hansen solubility parameters (δ_p; solubility parameter due to dipole forces, $MPa^{1/2}$) for different organic solvent molecules including protic polar solvents, aprotic polar solvents, and non-polar solvents. b) Graphical illustration of the polarity in membranes with confined pores enhancing the intramembrane selective transfer of polar/nonpolar solvent molecules.

differentiation. Some studies have leveraged the enhanced hydrophobicity of the membrane material to promote the passage of hydrocarbon solvents through the membrane.[10] Therefore, creating high-polarity membranes to separate solvents based on their polarity difference is feasible.

Currently, specific molecular building blocks, introduced via established interfacial polymerization (IP) techniques, are required for fundamental modifications of the structure and properties of the polyamide (PA) thin-film composite (TFC) membranes to enhance solvent mixture separation capabilities.[4b,11] Conventional TFC membranes constructed from the *m*-phenylenediamine (MPD) monomer exhibit favorable selectivity for desalination or solvent mixture separations due to their strong steric hindrance; however, they typically have low permeance of 0.03–0.3 L m^{-2} h^{-1} bar^{-1} for organic solvent mixtures.[1b,11a,12] Due to the tightly packed all-aromatic components and highly cross-linked structure of nascent PA membranes, with pore sizes ranging from 0.3 to 0.4 nm, the solvent separation performance depends primarily on strict pore-size regulation.[5,13] The characteristic of polarity in selective solvent transport is rarely utilized. In this regard, creating membranes with relatively large but limited pore sizes and highly polar pore surfaces may achieve both high permeance and selectivity. To realize this, amine monomers that are composed of abundant polar functional groups and flexible chains are ideal IP building blocks. Low-molecular-weight polyethyleneimine (PEI)[14] oligomers with aliphatic side chains and abundant amino groups are better for fabricating membranes with a highly polar and relatively loose PA layer than the MPD monomer. Specifically, the excess amino groups of PEI are necessary both for the IP reaction and as polar functional groups[15] that can remain in the polymer network to generate a high-polarity pore surface. In addition, PEI provides branched structures and flexible aliphatic chains in the polymer network, which contribute to the relatively low solvent transport resistance.[16]

Herein, PA layers embracing polar pore surfaces and relatively large pore sizes were fabricated using PEI and trimesoyl chloride (TMC) via interfacial polymerization. Another type of PA layer, featuring less polar pore surfaces and smaller pore sizes, was prepared using conventional MPD and TMC. A series of resulting PA TFC membranes with varying cross-linking degrees were fabricated under different conditions and tested, revealing a limitation to using the size exclusion effect to improve the solvent mixture separation performance. When the membrane pore size is reduced to below a certain threshold, further decreases lead to continued reduction in solvent permeance without significantly increasing selective solvent rejection. Comparisons between PEI-TMC and MPD-TMC membranes demonstrate that pore surface polarity can offset pore size limitations by enhancing membrane–solvent interactions, resulting in rapid and selective separation of solvent mixtures through a synergistic effect of pore size and polarity (Figure 1b). This work provides insights into regulating membrane polarity beyond pore size to enhance the separation performance of solvent mixtures in PA membranes.

2. Results and Discussion

2.1. Fabrication and Characterization of PA Membranes

In this study, oligomer PEI (600 g mol^{-1}) with rich amino groups was mainly applied as an aqueous-phase reactant to react with trimesoyl chloride (TMC) in hexane solution via IP on solvent-resistant polyketone (PK) substrates (**Figure 2**a; Figure S1, Supporting Information). The PEI-based PA network, compared to

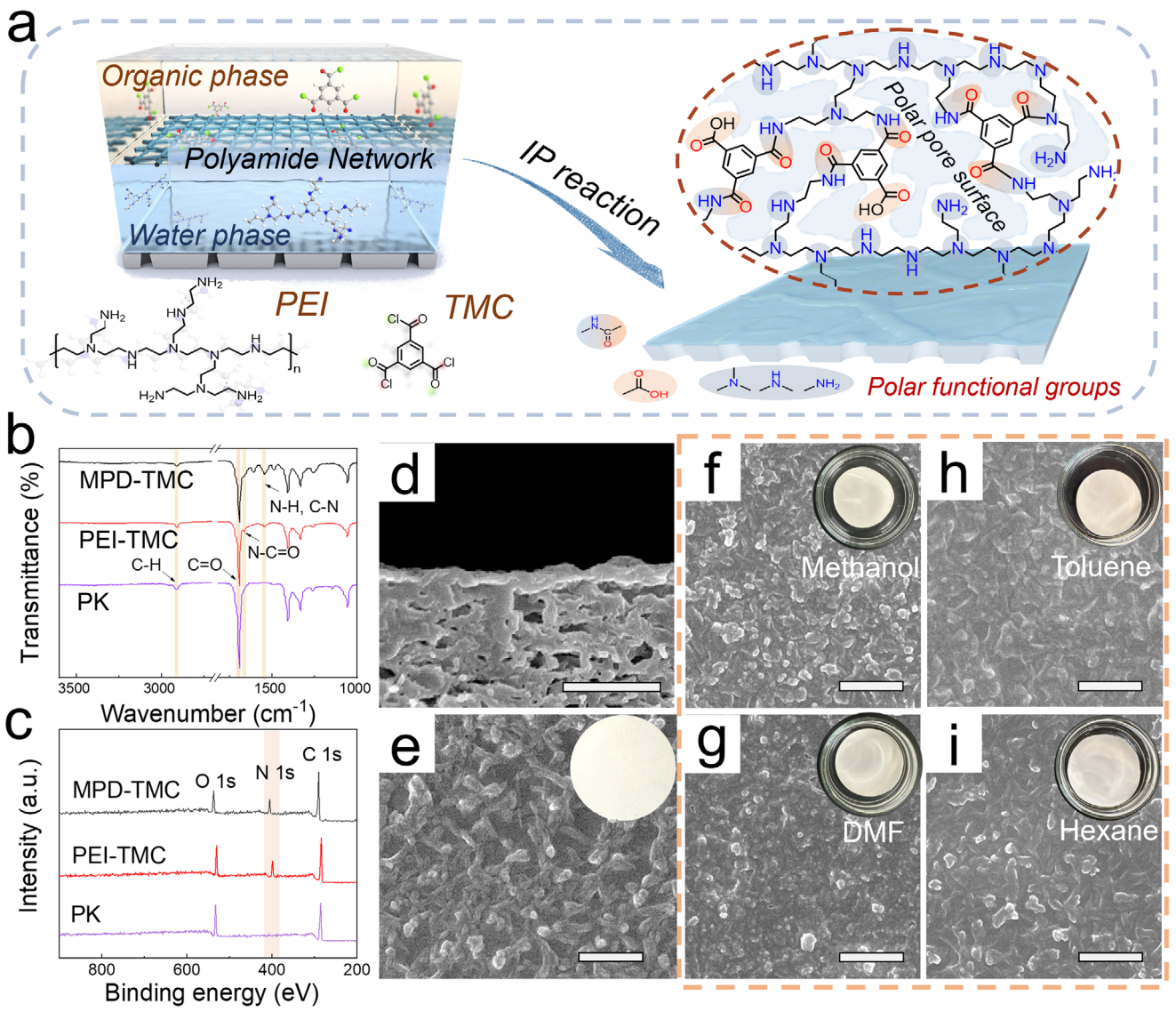

Figure 2. a) Schematic illustration of the IP reaction between PEI and TMC to construct a highly polar PA layer with abundant polar functional groups on the pore surface. b) FTIR, c) XPS spectra of PK substrate, MPD-TMC, and PEI-TMC membranes. d) Cross-section and e) surface morphology of the PEI-TMC membrane. The surface morphology of PEI-TMC membranes after soaking in f) methanol, g) DMF, h) toluene, and i) hexane for over 20 days. All scale bars represent 1 µm. Digital photos of the membranes are shown in the inset.

the MPD-based all-aromatic PA network, ideally has more polar functional groups and moderate steric hindrance (Figure S2, Supporting Information). The chemical structure and composition of the PA TFC membranes were analyzed by Fourier-transform infrared spectroscopy (FTIR) and X-ray photoelectron spectra (XPS). Characteristic peaks at 1663 and 1544 cm^{-1} in the FTIR spectra, attributed to the stretching vibration of C = O and C–N in the formed amide, confirmed the successful preparation of the PA layer (Figure 2b). In addition, the XPS result showed that, relative to the PK substrate, both PA TFC membranes exhibit a clear characteristic peak of N 1s at 400.8 eV, primarily ascribed to the formation of the PA layer (Figure 2c). This is further confirmed by the O = C–O (532.4 eV) and O = C–N (531.1 eV) peaks in the O 1s high-resolution spectra (**Figure 3a**; Figure S3, Supporting Information).

From scanning electron microscope (SEM) images showing the morphologies of different PA membranes (Figure 2d,e and Figure S4, Supporting Information), the PEI-TMC membrane exhibits a thin PA layer thickness and a smooth, dense surface with visible PK substrate fiber skeletons and minor nanoscale nodules, which is significantly different from the MPD-TMC membrane with typical ridge-and-valley surface morphology. Solvent resistance of the TFC membranes is a prerequisite for effective solvent separation. We immersed the PEI-TMC and MPD-TMC membranes in five typical types of solvents including polar protic methanol, polar aprotic dimethylformamide (DMF), and dimethyl sulfoxide (DMSO), nonpolar aromatic toluene, and nonpolar aliphatic hexane for more than 20 days to assess stability. The surface and cross-section morphology revealed that both TFC membranes remained intact and defect-free after

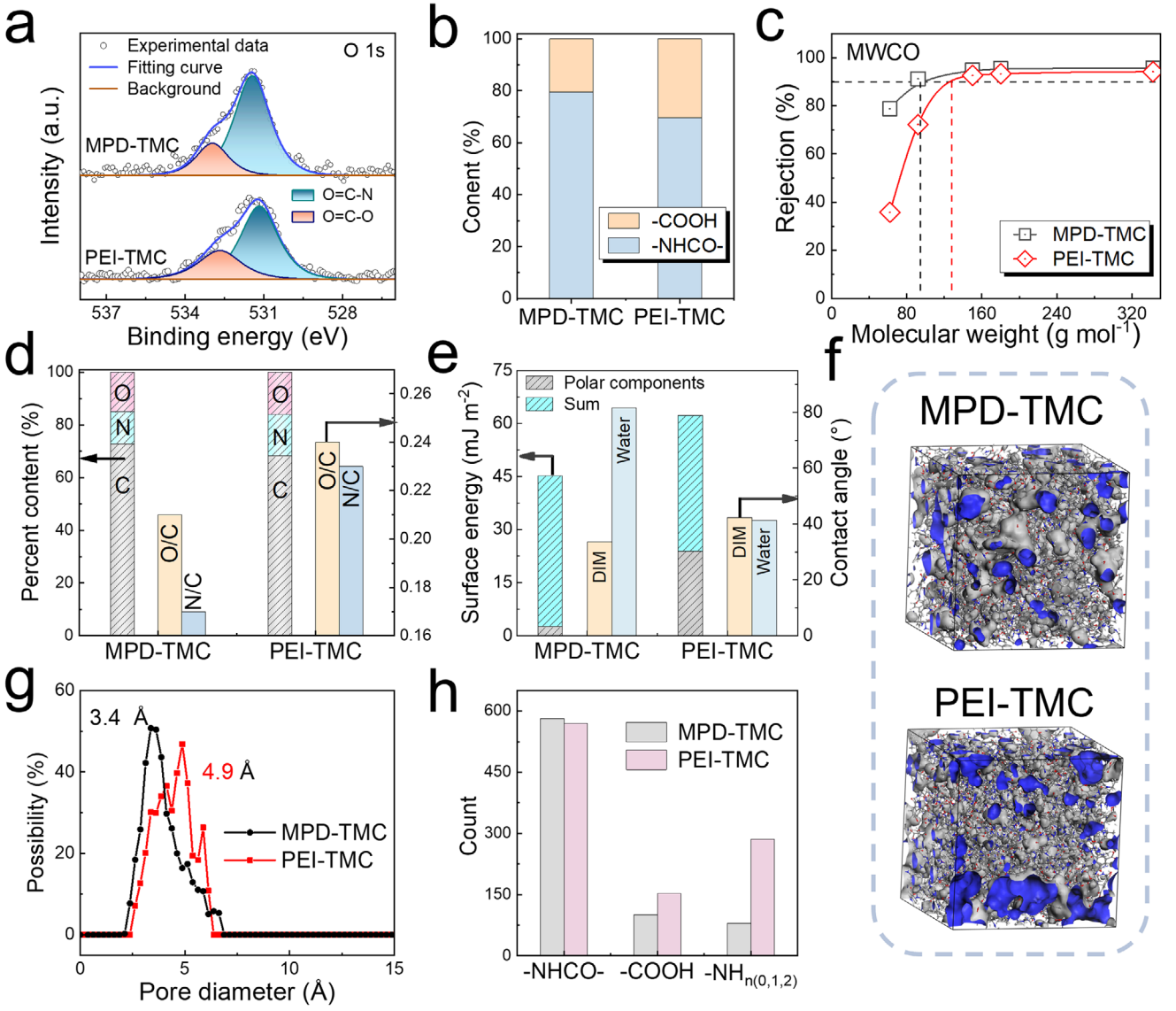

Figure 3. Physicochemical properties of PA TFC membranes: a) O 1s spectrum, b) percent content of amide bonds and carboxyl groups, c) MWCO profile using neutral solute rejection in water, d) content of the elements and the ratio of O/C and N/C, e) water and diiodomethane (DIM) contact angles, and surface energy of polar components (γ_s^p) for MPD-TMC and PEI-TMC membranes. Structural analysis based on MD simulations of MPD-TMC and PEI-TMC networks: f) 3D snapshots showing free volume distribution of the crosslinked amorphous models (Visualized using Materials Studio 2023. Grey color: surface of free volume at probe radius of 1.9 Å (Kinetic radius of methanol molecule); Blue color: surface of solvent accessible channels. Cell size: 4.4 × 4.4 × 4.4 nm^3), g) pore size distribution, and h) number of polar functional groups after crosslinking, including amide bonds, carboxyl groups, and unreacted amino groups.

solvent immersion, demonstrating the good solvent resistance of both PA and substrate layers in the TFC structures (Figure 2f–i; Figures S5 and S6, Supporting Information). The consistent characteristic peaks of the TFC membrane after immersion in various solvents demonstrate its chemical stability and structural integrity (Figure S7, Supporting Information).

2.2. Membrane Chemical Characterization

PEI-TMC and MPD-TMC membranes prepared under various conditions (Tables S2 and S3, Supporting Information) were selected for preliminary analyses of their cross-linked structures and membrane polarity (Tables S4–S7, Supporting Information). The PA was formed by the reaction between amine and acyl chloride, with its degree of cross-linking positively correlated to the content of amide bonds as determined by the XPS O 1s spectra (Figure 3a; Figure S8, Supporting Information). Since oxygen only comes from the acyl chloride groups of TMC, a higher amide bond content indicates greater cross-linking of acyl chloride with amines in the PA selective layer.[17] Unreacted acyl chloride will hydrolyze to carboxyl groups remaining in the PA. PEI-TMC membrane prepared under optimal conditions has a lower content of amide bonds (69.6%) compared to the MPD-TMC

membrane (79.6%), indicating a higher possibility of retaining more unreacted functional groups (Figure 3b). The pore size of both PA membranes under different IP times were also evidenced by the molecular weight cut-off (MWCO) tests (Figure S9 and Table S7, Supporting Information), where the PEI-TMC membrane prepared under optimal conditions has a higher MWCO (122.7 g mol^{-1}) than the MPD-TMC membrane (88.6 g mol^{-1}) (Figure 3c). The results are consistent with the theoretically proposed polymer network features.

A significant determinant of membrane polarity is the polar functional groups in the polymer structure of the membranes. These groups influence the dipole moment size of the polymer moieties, thereby affecting the polarity and intermolecular interactions. Thus, the polarity of polymers is primarily determined by the polar functional groups they have. More polar functional groups increase the overall dipole moment, resulting in higher polarity.[18] The polar groups of PA membranes include amide bonds (-CONH-), carboxyl groups (-COOH), and various amino groups ($-NH_{n(0,1,2)}$) (Figure S2, Supporting Information). Therefore, the polar functional group content of PA membranes can be compared by analyzing the relative O/C and N/C element ratios from XPS analysis. The results show that the O/C and N/C ratio of the PEI-TMC membrane is significantly higher than those of the MPD-TMC membrane (Figure 3d), indicating a higher membrane polarity. Furthermore, we analyzed the surface energy of the polar and dispersive components for two PA membranes using contact-angle data from water and diiodomethane (DIM) (Figure 3e; Figure S10 and Table S8, Supporting Information).[19] The data indicate that, compared to the MPD-TMC membrane (2.5 mJ m^{-2}), the polar component from the surface energy of the PEI-TMC membrane (23.8 mJ m^{-2}) is higher, further confirming its stronger membrane polarity. While different membrane preparation conditions caused slight variations in the polarity of PEI-TMC membranes, their values are significantly higher than MPD-TMC membranes (Figure S10, Supporting Information).

We performed molecular dynamic (MD) simulations on the cross-linking processes of both PA networks to analyze the pore structures and membrane polarity.[20] It was revealed that the crosslinked PEI-TMC network exhibited a large proportion of connected voids (blue regions) and thus high inner pore interconnectivity via inserting a theoretical probe of 1.9 Å radius (Figure 3f). Pore size distributions in Figure 3g calculated by MD simulations demonstrated that the substitution of MPD with the oligomer PEI permitted a significant increase in pore apertures from 3.4 Å to 4.9 Å within the 3D PA moiety. The theoretical pore size of the PEI-TMC membrane (4.9 Å) closely matches the experimental result (4.72Å) obtained through positron annihilation lifetime spectroscopy (PALS) (Figure S11, Supporting Information). In addition, the PEI-TMC network contains significantly more amino and carboxyl groups, with a slightly lower number of amide bonds compared to the MPD-TMC network, which suggests that PEI-TMC membranes have a more polar pore surface (Figure 3h; Figure S12, Supporting Information). The MD results validated our experimental observations, showing good agreement with the experimental data on MWCOs, XPS, and the surface energy of polar components.

2.3. Performance of PA TFC Membranes for Solvent Mixtures

The pore size of polymer membranes is usually determined by the cross-linked polymer network. A series of MPD-TMC and PEI-TMC membranes with varying degrees of cross-linking (amide bond content determined from the XPS O 1s spectra) (Figure S8 and Tables S2–S5, Supporting Information) were prepared using different preparation conditions. The results demonstrated that the amide bond content in the PA membranes increased with prolonged reaction time and higher amine monomer concentration (Figure S13, Supporting Information), indicating a greater degree of cross-linking. Pressurized methanol filtration through the membranes showed a decrease in methanol permeance as the degree of cross-linking increased (Figure S14a,b, Supporting Information). We also conducted filtration experiments (Figure S14c,d, Supporting Information) to study how the degree of cross-linking affects the separation performance of a solvent mixture composed of 95 wt.% methanol and 5 wt.% hexane, representing a mixture of polar and nonpolar solvents. A membrane with a smaller pore size (higher degree of cross-linking or higher content of amide bonds) shows higher rejection but a corresponding decrease in permeance (**Figure 4**a,b) for both PEI-TMC and MPD-TMC membranes. This demonstrates a typical trade-off effect between permeance and hexane rejection for both types of membrane materials, indicating the effective role of size exclusion in improving solvent separation by PA membranes.

We plotted the hexane rejection data against the corresponding membrane permeance for the series of MPD-TMC and PEI-TMC membranes with varying degrees of cross-linking. While both PEI-TMC and MPD-TMC membranes exhibit similar trade-off effects between permeance and rejection, they have different growth curves toward the maximum rejection (Figure 4c). Notably, while the PEI-TMC and MPD-TMC membranes both achieve a maximum hexane rejection of ≈97.5%, the PEI-TMC demonstrates significantly higher permeance (as indicated by the arrows in Figure 4a–c). A similar performance trend was also observed in the separation of methyl tert-butyl ether (MTBE)/methanol (Figure S15, Supporting Information). The results suggest that continuously increasing the degree of cross-linking of PA membranes will not achieve complete hexane rejection in methanol, likely due to the limited minimum pore size achievable with a PA membrane (Figure 4d), irrespective of whether it is PEI-TMC or MPD-TMC. However, a lower degree of cross-linking with a higher polar pore surface in PEI-TMC membranes can enable high permeance while maintaining similar levels of rejection to those recorded for MPD-TMC membranes, through a synergistic effect of polar pore surface and suitable pore size (Figure 4d). It is considered that the high polarity of the PEI-TMC membrane enhances repulsion between the PA layer and nonpolar hexane molecules, hindering their transmembrane transport, while increasing affinity with polar methanol molecules to facilitate transport (Figure 4d).

To verify the differential interactions between the membrane and solvent molecules, we used quartz crystal microbalance with dissipation (QCM-D) sensors coated with PEI-TMC and MPD-TMC membrane films (Figure 4e). These were installed in a flow cell to characterize the affinity (adsorption capacity)

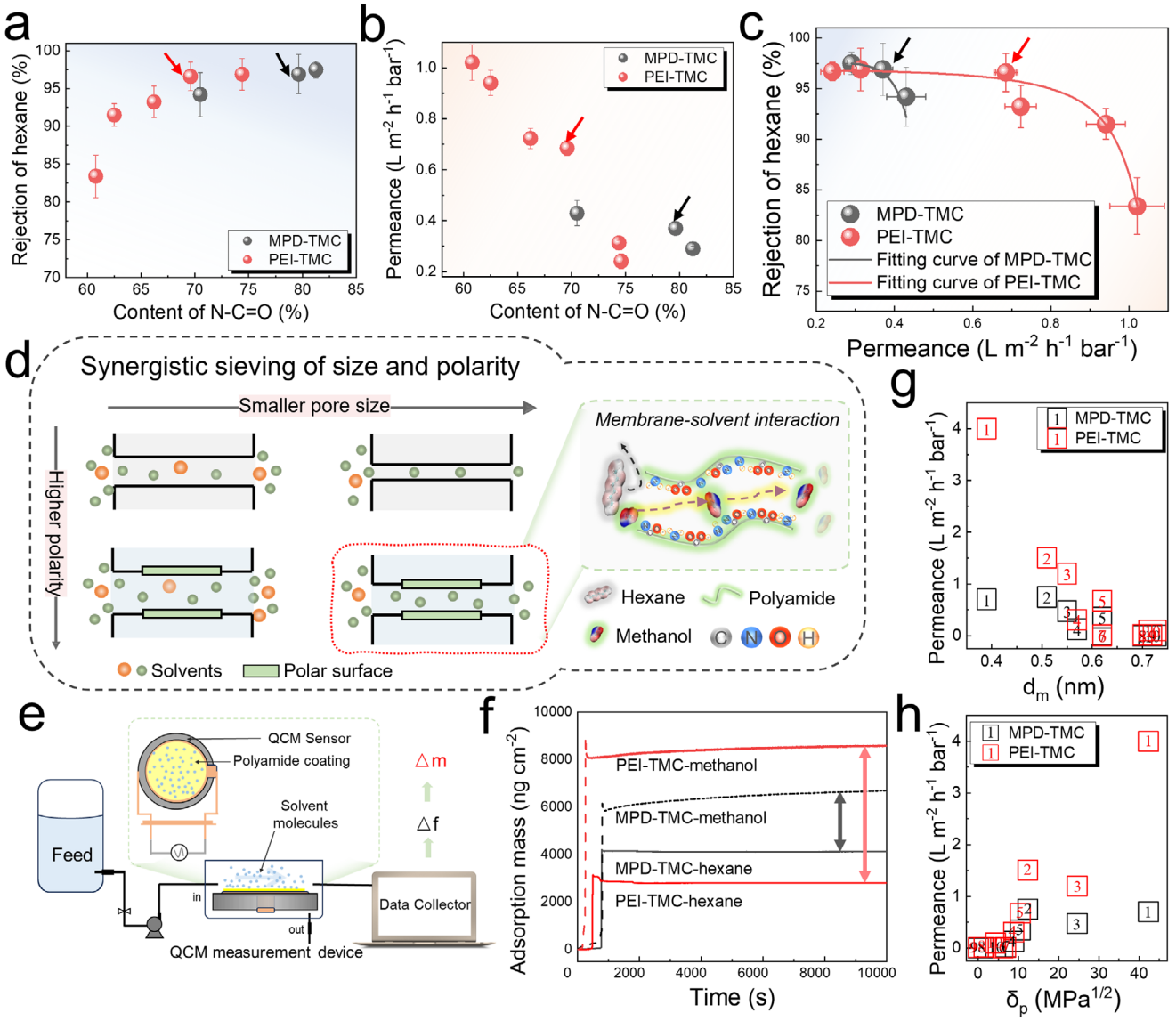

Figure 4. Performance of PA TFC membranes. a) Hexane rejection and b) total permeance of PA membranes with different degrees of cross-linking (the content of N–C = O obtained from the XPS O 1s spectra). c) Trade-off effect between total permeance and hexane rejection by PA membranes including the PEI-TMC membrane prepared under different IP times and PEI concentrations, as well as the MPD-TMC membrane prepared under different IP times. Feed concentration of hexane/methanol is 5/95 (w/w). d) A schematic illustrating the mechanism of how pore size and polarity affect separation performance, along with the interaction between a polar pore surface and polar/nonpolar solvents. e) Schematic diagram of QCM-D test. f) Adsorption mass of methanol and hexane of MPD-TMC and PEI-TMC membranes was measured by QCM-D. The relationship between solvent permeance and solvent properties including g) molar diameter (d_m, nm) and h) Hansen solubility parameter (δ_p; solubility parameter due to dipole forces, $MPa^{1/2}$). The solvent sequence: water (1), methanol (2), acetonitrile (3), ethanol (4), acetone (5), isopropanol (IPA) (6), *n*-propanol (7), toluene (8), hexane (9), MTBE (10). Error bar represents the standard deviation of triplicate measurements.

of the PA membranes with methanol (polar) and hexane (nonpolar) solvents, as shown in Figure 4f.[21] The results indicate that although both PEI-TMC and MPD-TMC membranes exhibit higher methanol affinity than hexane, PEI-TMC membranes exhibit a significantly larger affinity difference between methanol and hexane. This further demonstrates that the high polarity of the PEI-TMC membrane likely leads to significantly different interactions with polar and nonpolar solvent molecules during their transport, resulting in differentiated transmembrane behavior.

Using the representative PEI-TMC and MPD-TMC membranes with similar rejection capabilities above, the dependence of solvent transport on molecular size (molar diameter, d_m) and polarity (Hansen solubility parameter related to dipole forces, δ_p) was further examined through solvent permeation tests with different solvents (Figure 4g,h; Table S9, Supporting Information). The results indicate that the solvent transport rate generally depends on its size and polarity, with smaller and more polar solvents being transported faster. PEI-TMC membrane exhibited higher permeance for polar solvents compared to the MPD-TMC

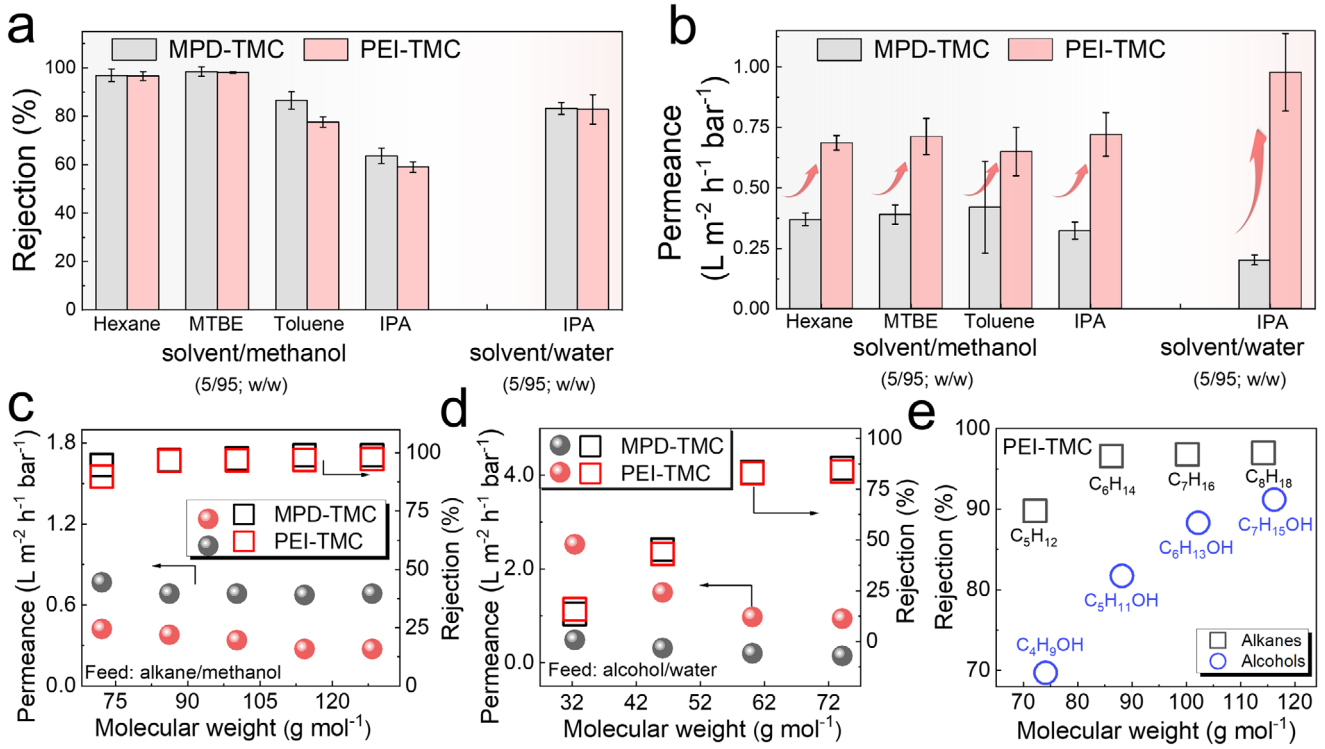

Figure 5. Comparison of a) the rejection and b) the total permeance of MPD-TMC and PEI-TMC membranes toward various solvent mixtures including hexane, MTBE, toluene, and IPA in methanol, as well as IPA in water. Separation performance of binary solvent mixtures including c) linear alkane/methanol and d) linear alcohol/water. e) Rejection of linear alcohols and linear alkanes with approximate molecular weights in methanol by PEI-TMC membranes. Feed concentration of solvent/methanol is 5/95 (w/w). Feed concentration of solvent/water is 5/95 (w/w). Error bar represents the standard deviation of triplicate measurements.

membrane. Additionally, we analyzed the permeance data using combined solvent properties to assess their linear fit with the typical solvent transport model in OSN. Compared to MPD-TMC membranes, PEI-TMC membranes demonstrated a stronger linear fit, particularly for strongly polar solvents (Figure S16, Supporting Information).

Further solvent mixture separation was carried out using the optimized representative PEI-TMC and MPD-TMC membranes. Methanol-based binary solvent mixtures with hexane, MTBE, toluene, or IPA as well as a water-based binary solvent mixture with IPA were used as feed for the tests. The results show that the PEI-TMC membrane has a similar solvent rejection profile to that of the MPD-TMC membrane but with significantly higher permeance (**Figure** 5a,b). Specifically, compared to the MPD-TMC membrane, the PEI-TMC membrane achieved a similar rejection of 97.5% for hexane and 98% for MTBE from their methanol mixtures, but increased permeance by 86.5% and 82.3%, respectively. Such effects were more pronounced when a water-based binary solvent mixture was used for separation. Compared to the IPA/methanol mixture, IPA rejection in the IPA/water mixture is higher for both membranes due to the greater polarity difference between water and IPA than between methanol and IPA. Notably, the permeance of the PEI-TMC membrane with the water/IPA mixture is ≈5 times that of the MPD-TMC membrane. These results further highlight the contribution of polar pore surfaces in membranes for the efficient separation of solvents with polarity differences. Consistent results were also found for the separation of methanol-based binary solvent mixtures of other linear alkanes (Figure 5c), aromatics (Figure S17a, Supporting Information), alcohols (Figure S17b, Supporting Information), and water-based binary solvent mixtures of polar protic alcohols (Figure 5d) and other polar aprotic solvents (Figure S18, Supporting Information) using both membranes.

To highlight polarity-based separation, we compared the rejection of linear alkanes (C_nH_{2n+2}) and linear alcohols ($C_{n-1}H_{2n+2}O$) in methanol-based binary solvent mixtures (Figure 5e). Specifically, although pentane (C_5H_{12}) and butanol ($C_4H_{12}O$) have similar molecular weights, sizes, and structures, the rejection of pentane from methanol was significantly higher than that of butanol. Similar trends were observed for hexane versus pentanol, heptane versus hexanol, and octane versus heptanol; in all cases, alkane rejection was consistently higher than that of the corresponding alcohols with similar molecular weights. This indicates that a larger polarity difference between solvents in a mixture enhances separation by PA membranes with polar pore surfaces.

Additional solvent mixture separation experiments were performed using the PEI-TMC membrane. When fed with a multicomponent solvent mixture consisting of methanol (97.5 mol%) and various linear alkanes (each 0.5 mol%), the membrane effectively purified methanol by rejecting most alkanes, as seen from the gas chromatogram of feed and permeate samples (**Figure** 6a). The result showed that methanol, as the primary contributor to permeance, is almost entirely concentrated in the permeate since almost no peaks other than methanol were observed in the

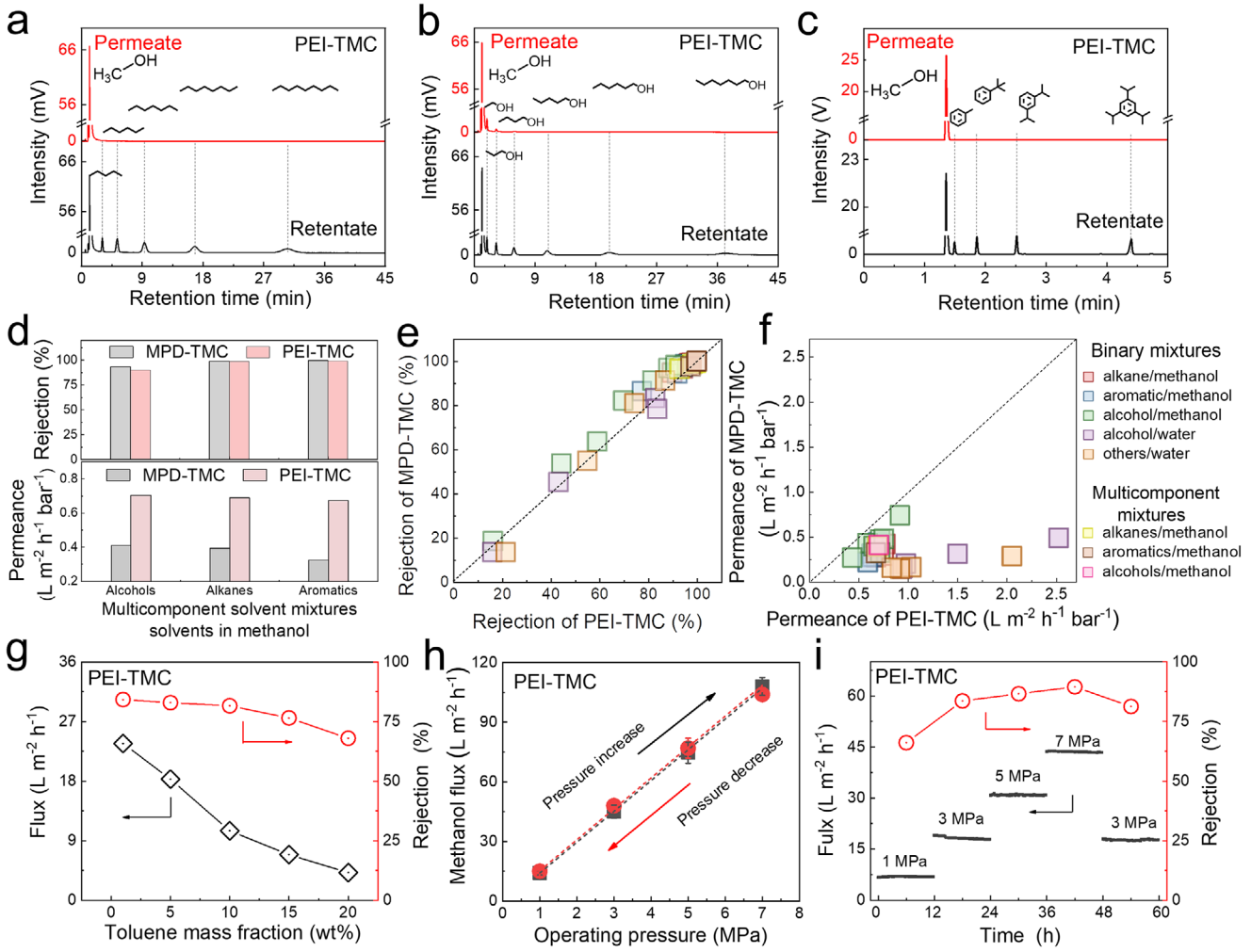

Figure 6. Separation performance of the PEI-TMC membrane for multicomponent solvent mixtures, including a) alkanes/methanol and b) alcohols/methanol determined with a thermal conductivity detector, and c) aromatics/methanol determined with a flame ionization detector. d) The total rejection and permeance of alcohols, alkanes, and aromatics in methanol by MPD-TMC and PEI-TMC membranes. Comparison of solvent mixture separation performance including e) rejection and f) total permeance between PEI-TMC and MPD-TMC membranes (the *x*- and *y*-axis represent PEI- and MPD-TMC membranes, respectively). g) Separation performance of PEI-TMC membrane for toluene/methanol mixtures with different toluene concentrations. h) The pure methanol flux of PEI-TMC membrane with increasing pressure from 1 to 7 MPa and then decreasing pressure to 1 MPa. i) Filtration stability of the PEI-TMC membrane for toluene/methanol mixtures under variable pressure operation. Error bar represents the standard deviation of triplicate measurements.

permeate. This trend is consistent with the filtration test results using a multicomponent methanol mixture containing various aromatics or alcohols (Figure 6b,c). In addition, the PEI membrane demonstrated high rejection for multicomponent alkanes, aromatics, and alcohols with different molecular weights, comparable to those of the MPD-TMC membrane but with higher permeance (Figure 6d; Figure S19, Supporting Information).

To visually demonstrate the significant potential of the PEI-TMC membranes with high polar pore surfaces for separating organic media, we used a 2D coordinate system to correlate the total permeance and rejection of MPD-TMC and PEI-TMC membranes for 24 different binary solvent mixtures and 3 different multicomponent solvent mixtures. The *x*-axis of Figure 6e,f represents the rejection or permeance of the PEI-TMC membrane, while the *y*-axis represents that of the MPD-TMC membrane. The straight dashed lines in the plots represent the diagonal line $y = x$, on which the rejection or permeance of the two membranes is the same. Most data points in Figure 6e are close to the line of $y = x$, indicating that PEI-TMC membranes have a similar rejection to MPD-TMC membranes for these solvent mixtures (Figure 6e). In addition, the data points in Figure 6f are mostly in the region of $x > y$, indicating that the PEI-TMC membrane generally has higher permeance than the MPD-TMC membrane. This reveals that the PEI-TMC membranes maintain a comparable rejection capability to the MPD-TMC membranes but exhibit significantly higher permeance. The permeability advantage of the PEI-TMC membrane is also evident when compared to other reports (Table S10, Supporting Information).

Toluene rejection from methanol is relatively low (<90%) for PA membranes compared to other nonpolar solvents (>95%),

likely due to its smaller molecular volume and slightly weaker polarity. Using this mixture would make it clearer to observe the change in separation performance upon changes of the operating conditions. Figure 6g indicates that the total flux and rejection of PEI-TMC membranes decreased with increasing toluene concentration from 1 to 20 wt.%. This performance trend is also presented in the MPD-TMC membranes of Figure S20 (Supporting Information). Given the direct proportionality between solute concentration and osmotic pressure in the mixture, the effective pressure for solvent molecules to cross the membrane decreases with increasing feed concentration, resulting in reduced flux (Figure S21, Supporting Information).[21a] The decreased rejection level is mainly due to slower transport of methanol resulting from the decreased effective pressure and concentration polarization caused by the accumulation of more toluene on the membrane surface.[22]

To evaluate the durability of the PEI-TMC membranes, filtration tests using pure methanol and methanol/toluene solvent mixtures under various pressure conditions were performed. The results demonstrated that pure methanol flux increased linearly with raised pressure from 1 to 7 MPa and maintained the same performance when the pressure was reduced from 7 to 1 MPa (Figure 6h). For separating methanol/toluene solvent mixtures at 3 MPa during both pressure increase and decrease stages, the PEI-TMC membrane maintained a consistent total flux (≈18 L m^{-2} h^{-1}) and toluene rejection (≈80%) (Figure 6i). This indicates that the PA layer of the PEI-TMC membrane exhibits operational stability under varying pressure conditions. A similar performance trend was found for the MPD-TMC membrane but with a lower solvent flux (Figure S22, Supporting Information). The rejection of toluene by PEI-TMC membranes was elevated with increasing pressure since the increase in methanol flux with pressure was much higher than that of toluene (Figure S23, Supporting Information).

In summary, the relatively large pore size of the PEI-TMC membrane enhances transmembrane transport, while its polar pore surface strengthens differential interactions with solvents of different polarities. This combination allows for rapid and selective separation of mixed solvents with a polarity difference. Thus, the synergistic effects of polarity and size sieving from a PA membrane with a polar pore surface can overcome the trade-off limitations of relying solely on size effect.

3. Conclusion

In this work, we confirmed the important role of a polar pore surface in a PA membrane for separating mixed solvents with polarity differences. By coupling a high-polarity pore surface with suitably large pore size, the PA membrane mitigates the limitation of sacrificing selectivity for permeability that is inherent to systems using size sieving alone and can enable both comparable selectivity and enhanced permeability. The results reveal that membrane polarity can generally compensate for the selectivity loss from size sieving and improve solvent permeance while maintaining a similar solvent rejection capability.

Solvent transport through membranes is influenced not only by pore geometry but also by pore surface chemistry, such as hydrophilicity and polarity. Utilizing the pore surface chemistry can offset the limitations in pore-size control, achieving more efficient separations. Understanding polymer–solvent interactions can advance pressure-driven solvent mixture separation membrane technology, contributing to more sustainable and efficient separation processes. Although membrane separations do not yet match the separation precision of thermal-based distillation, they offer significant advantages in applications such as solvent concentration and purification, such as concentrating IPA or DMF in water.[22,23] We recognize that some solvent mixtures (e.g., toluene in methanol) are not separated with high precision, necessitating further adjustments to optimize the synergistic effect of pore size and polarity. In addition, high operational pressures are required due to the high osmotic pressure of solvent mixtures, which may compromise the energy efficiency of the membrane process and thus call for new approaches such as osmosis-assisted reverse osmosis. Nonetheless, controlling pore surface chemistry can lead to more efficient solvent separation through pressurized membrane filtrations, providing useful information for the design of membranes for solvent mixture separations.

4. Experimental Section

Fabrication of Polyketone (PK) Substrate: The PK substrate was prepared through the conventional nonsolvent-induced phase separation (NIPS) method. A casting solution was formed by dissolving PK powder (14 wt.%) in resorcinol and deionized (DI) water mixture (35/65; w/w) at 80 °C, which was stirred for 8 h then degassed overnight at 60 °C. The solution was cast onto a non-woven fabric (casting gap: 400 µm). After immersing in a methanol/water coagulation bath (35/65; w/w) for 20 min, the membrane was washed in acetone and hexane (20 min each). The resulting PK membrane was air-dried and stored for further use.

Fabrication of PA TFC Membranes: The PEI-TMC membrane was prepared via conventional IP on a PK substrate, utilizing the reaction between PEI and TMC. The PK substrate was prewetted with a 3.5 wt.% PEI aqueous solution for 5 min, then the excess solution was removed with a rubber roller. Subsequently, a TMC solution (0.15 wt.%) in hexane was applied to the PEI-impregnated side for the IP reaction. The resulting membranes were cured at 100 °C for 3 min and stored in DI water. MPD-TMC membranes were prepared under the same IP conditions by replacing the PEI with MPD. The designated labels and corresponding IP parameters of the synthesized TFC membranes are summarized in Tables S1 and S2 (Supporting Information).

Filtration Performance Measurement: The separation performance of PA TFC membranes for solvent mixtures was tested at 25 °C via a homemade cross-flow setup with a filtration area of 7.1 cm^2 and a flow rate of 60 mL min^{-1} (Figure S24, Supporting Information). PA TFC membranes were pre-compacted with methanol filtration at 30 bar for 12 h to ensure recorded weight change of permeate reached a steady state. The separation performance of solvent mixtures was then tested at same conditions. The permeance (P, L m^{-2} h^{-1} bar^{-1}) was determined using the Equation (1):

$$P = \frac{V}{A \times \Delta P \times \Delta t} \quad (1)$$

where P (L m^{-2} h^{-1} bar^{-1}) is the permeance, V (L) represents the permeate volume during operational time Δt (h), A (m^2) represents the filtration area, and ΔP (bar) is the applied pressure.

For solvent mixture tests, alcohol/methanol, alkane/methanol, aromatic/methanol, and solvent/water were used. The rejection of solvent in methanol was calculated by analyzing the content of feed and permeate using gas chromatography (GC-2020, Shimadzu Corp., Kyoto, Japan and GC-2030, Shimadzu Corp., Kyoto, Japan). The mixtures of alkane/methanol and alcohol/methanol were analyzed with a thermal conductivity detector, and the mixtures of aromatics /methanol were analyzed with a flame

ionization detector. The rejection of solvent in water was calculated by measuring the refractive index of feed and permeate using an Abbe refractometer (NAR-1T, ATAGO Co. Ltd., Tokyo, Japan). The rejection of the prepared membranes was obtained from Equation (2):

$$R = \left(1 - \frac{C_P}{C_F}\right) \times 100\% \quad (2)$$

where R (%) is the rejection, C_P and C_F represent the rejected solvent concentrations of the permeate and feed fluids of solvent mixtures, respectively.

QCM-D Measure Method: In the QCM-D technique, a voltage is applied to a quartz crystal, causing it to oscillate at a specific frequency due to the piezoelectric effect. Changes in the sample mass on the quartz surface led to measurable frequency shifts (f) of the oscillating crystal through the Sauerbrey equation. Therefore, QCM-D was employed to quantify small changes in solvent adsorption on the PA membranes.[24] First, the samples were prepared by constructing free-standing PA membranes of PEI-TMC and MPD-TMC at the water/*n*-hexane interface under the optimized conditions. These membranes were then transferred onto the surface of the gold-coated sensor and vacuum-dried. Next, the as-prepared sensor sample was sealed in the flow cell of QCM-D setup. The adsorption process of methanol and *n*-hexane solvents on PA membranes was tested using a low-flow-rate cross-flow method. The change in mass due to the adsorption of solvent was calculated using the Equations (3) and (4):

$$\Delta m = \frac{-C \times \Delta f}{n} \quad (3)$$

$$C = \frac{t_q \times \rho_q}{f_0} \quad (4)$$

where Δm is the mass of the adsorbed solvent, Δf is the difference of moisture, n is the overtone. C is a constant value (17.7 ng $Hz^{-1}cm^{-2}$), which was calculated using Equation (4), where t_q is the thickness of the quartz crystal and ρ_q is the density of the quartz crystal. The crystal was excited at its fundamental frequency (f_0) of ~5 MHz, with Δf monitored at both the fundamental ($n = 1$) and overtone frequencies ($n = 3$, 5, 7, 9, and 11). The data reported here were derived from the fifth overtone ($n = 5$), as readings at the fundamental frequency are often excluded due to artifacts caused by the sensor clamp.

Statistical Analysis: The data with error bar are presented as means ± standard deviation, with error bars indicating the standard deviation of triplicate measurements.

Supporting Information

Supporting Information is available from the Wiley Online Library or from the author.

Acknowledgements

A.Z. thanks the China Scholarship Council (No. 202307040020) for financial support.

Conflict of Interest

The authors declare no conflict of interest.

Author Contributions

H.M., K.G., and A.Z. conceived the idea, and designed the research and experiments. A.Z. carried out the experiments and analyzed the data including membrane fabrication, characterization, and performance tests. Z.M. carried out MD simulations. Z.W., Z.L., L.D., C.L., B.L., M.H., and P.Z. provided constructive suggestions for results and discussion. A.Z., K.G., and H.M. wrote and revised the manuscript.

Data Availability Statement

The data that support the findings of this study are available from the corresponding author upon reasonable request.

Keywords

interfacial polymerization, membrane-solvent interactions, polar pore surfaces, polyamide membranes, solvent mixture separation

Received: November 17, 2024
Revised: January 6, 2025
Published online:

[1] a) H. Sun, F. Wang, X. Li, J. Caro, H. Meng, N. Wang, Q. F. An, *Angew. Chem., Int. Ed.* **2023**, *135*, 202300262; b) C. Liu, G. Dong, T. Tsuru, H. Matsuyama, *J. Membr. Sci.* **2021**, *620*, 118882.
[2] D. S. Sholl, R. P. Lively, *Nature* **2016**, *532*, 435.
[3] R. P. Lively, D. S. Sholl, *Nat. Mater.* **2017**, *16*, 276.
[4] a) C. Liu, G. Dong, T. Tsuru, H. J. J. o. M. S. Matsuyama, *J. Membr. Sci.* **2021**, *620*, 118882; b) B. Liang, X. He, J. Hou, L. Li, Z. Tang, *Adv. Mater.* **2019**, *31*, 1806090.
[5] Z. Ali, B. S. Ghanem, Y. Wang, F. Pacheco, W. Ogieglo, H. Vovusha, G. Genduso, U. Schwingenschlögl, Y. Han, I. Pinnau, *Adv. Mater.* **2020**, *32*, 2001132.
[6] a) B. Van der Bruggen, J. Schaep, D. Wilms, C. J. J. o. M. S. Vandecasteele, *J. Membr. Sci.* **1999**, *156*, 29; b) D. R. Machado, D. Hasson, R. Semiat, *J. Membr. Sci.* **2000**, *166*, 63.
[7] C. M. Hansen, *Hansen Solubility Parameters: A User's Handbook*, CRC press, Boca Raton, Florida **2007**.
[8] B. Van der Bruggen, J. Geens, C. Vandecasteele, *Chem. Eng. Sci.* **2002**, *57*, 2511.
[9] a) A. F. J. C. R. Barton, *Chem. Rev.* **1975**, *75*, 731; b) Y. Marcus, in *Solvent Extraction Principles and Practice, Revised and Expanded*, CRC press, Boca Raton, Florida **2004**, p. 37; c) X. Zhang, T. Li, Z. Wang, J. Wang, S. Zhao, *J. Membr. Sci.* **2023**, *668*, 121294; d) B. Zhuang, G. Ramanauskaite, Z. Y. Koa, Z.-G. Wang, *Sci. Adv.* **2021**, *7*, eabe7275.
[10] a) S. Li, R. Dong, V.-E. Musteata, J. Kim, N. D. Rangnekar, J. Johnson, B. D. Marshall, S. Chisca, J. Xu, S. Hoy, *Science* **2022**, *377*, 1555; b) W. Kushida, R. R. Gonzales, T. Shintani, A. Matsuoka, K. Nakagawa, T. Yoshioka, H. Matsuyama, *J. Mater. Chem. A* **2022**, *10*, 4146.
[11] a) K. Guan, S. Fang, S. Zhou, W. Fu, Z. Li, R. R. Gonzales, P. Xu, Z. Mai, M. Hu, P. Zhang, *J. Membr. Sci.* **2023**, *688*, 122104; b) Y. Li, Z. Guo, S. Li, B. Van der Bruggen, *Adv. Mater. Interfaces* **2021**, *8*, 2001671; c) L. Deng, R. R. Gonzales, W. Fu, G. Xu, R. Takagi, Q. Song, S. Zhou, H. Matsuyama, *Chem. Eng. J.* **2023**, *473*, 145197; d) A. Zhang, J. Zhu, S. Han, Y. Zhang, B. Van der Bruggen, *J. Membr. Sci.* **2022**, *662*, 120987.
[12] a) Q. Gan, L. E. Peng, H. Guo, Z. Yang, C. Y. Tang, *Environ. Sci. Technol.* **2022**, *56*, 10308; b) W. Fu, M. Hu, J. Liu, L. Deng, K. Guan, R. R. Gonzales, S. Fang, Z. Wang, Y. Shi, S. Xiang, *J. Membr. Sci.* **2024**, *704*, 122901.
[13] a) Z. Ali, Y. Wang, W. Ogieglo, F. Pacheco, H. Vovusha, Y. Han, I. Pinnau, *J. Membr. Sci.* **2021**, *618*, 118572; b) T. H. Lee, M. Balcik, W.-N. Wu, I. Pinnau, Z. P. Smith, *Sci. Adv.* **2024**, *10*, eadp6666.
[14] a) F. Zhao, Y. Mi, Q. An, C. Gao, *Prog. Chem.* **2016**, *28*, 541; b) A. El Fadil, E. Bull, M. Bastin, R. Verbeke, S. R. Hosseinabadi, S. Eyley, W. Thielemans, K. Nijmeijer, I. F. Vankelecom, *J. Membr. Sci.* **2023**, *685*,

121862; c) L. Zhang, G. He, W. Zhao, F. Nie, X. Li, M. Tan, *J. Membr. Sci.* **2011**, *371*, 141.
[15] M. Namvar-Mahboub, M. Pakizeh, *Sep. Purif. Technol.* **2013**, *119*, 35.
[16] a) C. Wang, M. J. Park, R. R. Gonzales, S. Phuntsho, H. Matsuyama, E. Drioli, H. K. Shon, *J. Membr. Sci.* **2022**, *655*, 120582; b) M. R. S. Kebria, M. Jahanshahi, A. Rahimpour, *Desalination* **2015**, *367*, 255.
[17] a) P. Li, H. Lan, K. Chen, X. Ma, B. Wei, M. Wang, P. Li, Y. Hou, Q. J. Niu, *Sep. Purif. Technol.* **2022**, *280*, 119949; b) S. Li, R. Zhang, Q. Yao, B. Su, L. Han, C. Gao, *Sep. Purif. Technol.* **2022**, *286*, 120496.
[18] a) A. W. Trochimczuk, M. Streat, B. N. Kolarz, *React. Funct. Polym.* **2001**, *46*, 259; b) S. R. Holmes-Farley, C. D. Bain, G. M. J. L. Whitesides, *Langmuir* **1988**, *4*, 921.
[19] a) J. Carpenter, H. Kim, J. Suarez, A. Van Der Zande, N. Miljkovic, *ACS Appl. Mater. Interfaces.* **2022**, *15*, 2429; b) F. M. J. T. J. o. P. C. Fowkes, *J. Phys. Chem.* **1963**, *67*, 2538.
[20] T. Wei, L. Zhang, H. Zhao, H. Ma, M. S. J. Sajib, H. Jiang, S. Murad, *J. Phys. Chem. B* **2016**, *120*, 10311.
[21] a) W. Fu, M. Hu, J. Liu, L. Deng, K. Guan, R. R. Gonzales, S. Fang, Z. Wang, Y. Shi, S. Xiang, *J. Membr. Sci.* **2024**, *704*, 122901; b) L. Dai, F. Xu, K. Huang, Y. Xia, Y. Wang, K. Qu, L. Xin, D. Zhang, Z. Xiong, Y. Wu, *Angew. Chem., Int. Ed.* **2021**, *133*, 20086.
[22] Y.-H. Chiao, Z. Mai, W.-S. Hung, H. Matsuyama, *J. Membr. Sci.* **2023**, *672*, 121434.
[23] M. Hu, K. Kumagai, R. R. Gonzales, Y.-H. Chiao, K. Guan, T. Kawakatsu, H. Matsuyama, *J. Membr. Sci.* **2024**, *697*, 122581.
[24] a) W. Fu, M. Hu, J. Liu, L. Deng, K. Guan, R. R. Gonzales, S. Fang, Z. Wang, Y. Shi, S. Xiang, P. Zhang, W. Shi, H. Matsuyama, *J. Membr. Sci.* **2024**, *704*, 122901; b) L. Dai, F. Xu, K. Huang, Y. Xia, K. Qu, X. Guo, W. Jin, Z. Xu, *Angew. Chem., Int. Ed.* **2021**, *60*, 19933.